CrystEngComm

Accepted Manuscript

ROYAL SOCIETY OF CHEMISTRY

www.rsc.org/crystengcomm

Journal Name

ARTICLE

The Role of Polarity and Surface Energy in the Growth Mechanism of ZnO from Nanorods to Nanotubes

Received 00th January 20xx,
Accepted 00th January 20xx

DOI: 10.1039/x0xx00000x

www.rsc.org/

Kwong-Lung Ching*, Guijun Li, Yeuk-Lung Ho, Hoi-Sing Kwok*

The polarity of zinc oxide nanostructures is crucial to modern electronic devices in terms of electrical and optical properties. However, it is still unclear whether the growth direction which affects the polarity of zinc oxide nanorods in hydrothermal processes in Zn-, O- or mix-polar. Earlier studies suggested it should be Zn-polar based in the thermodynamic calculation. Later, studies propose that the nanorods are O-polar, i.e. less stable than Zn-polar, resulting in the formation of nanotubes by KOH etching. Recently, the possibility of the co-existence of both Zn- and O-polar has been demonstrated. Therefore, we investigated the polarity issue, by fabricating two types of ZnO nanorods in acidic and alkaline growth conditions. The as-grown and etched morphologies of these two types of nanorods are obviously different. Valence band x-ray photoemission spectroscopy (VB-XPS) has been employed to determine the polarity. We found that nanorods from both conditions are Zn-polar. This led us to find out the formation of nanotubes is determined by the surface energy on the Zn-polar face of heterogeneously grown nanorods. The surface energy of ZnO nanorods can be controlled by a second acidic chemical bath, as long as the surface is not annealed. Furthermore, the thermodynamics of the process was studied to investigate the possible growth mechanism after the confirmation of polarity.

KEYWORDS: ZnO nanorods, polarity, surface energy, VB-XPS, thermodynamics

Introduction

ZnO has been intensively studied because of its controllable morphology, high optical transparency and good electrical properties. It has been widely applied in electroluminescent devices[1], OLED[2], spintronic[3], thin film transistors[4], nanogenerators[5], and photovaltaic[6]. For modern nano-electronic devices, a variety of different nanostructures such as nanowires[1], nanorods[6], nanorings[7] and nanotubes[8] can be produced by a low temperature hydrothermal method. One of the advantages of the hydrothermal method is cost-effectiveness, without the need of high vacuum and high temperature, thus being amenable for mass production. In the hydrothermal method, zinc oxide usually forms a hexagonal wurtzite structure where each Zn atom is surrounded by four O atoms, and vice versa, to form the ZnO_4^{6-} tetrahedron. It belongs to the space group C_{6v}^4 in the Schoenflies notation, and $P6_3mc$ in the Hermann-Mauguin notation. This consists of alternative layers of Zn and O atoms, and the resulting crystal has a Zn-polar plane (0001) and an O-polar plane ($000\bar{1}$), as shown in Figure 1a. Besides having six non-polar faces, the zinc oxide is a polar crystal which has the positive charged Zn-polar surface and the negative charged O-polar surface. These are terminated respectively by Zn and O atoms, as shown in Figure 1b. The positive and negative charged ZnO faces are very important in the growth mechanism of electrostatic attraction.[9]

The polarity of ZnO affects many properties such as photoluminescence[10], the barrier height of Schottky contact[11] and surface energy[12,13], which are vital factors for designing the modern electronic devices. However, the academic debate concerning the polarity is still ongoing in that there are three conflicting proposals. First, Li et al.[14] and Laudise et al.[15] proposed that the speed of growth directions in Zn-polar was greater than in O-polar for the homogeneously-grown nanorods. Then, a detailed thermodynamic study of the Zn-NH_3-OH system was done by Richardson and Lange[16] and others[1,17-19], who proposed that the electrostatic attraction

State Key Laboratory on Advanced Displays and Optoelectronics Technologies, Department of Electronic and Computer Engineering, Hong Kong University of Science and Technology, Clear Water Bay, Hong Kong. Email: klching@ust.hk;eekwok@ust.hk

Electronic Supplementary Information (ESI) available: The SEM images of as-grown and KOH etched nanorods of acidic growth conditions are shown in Figure S1, the SEM images of as-grown and KOH etched nanorods of alkaline growth conditions are shown in Figure S2, the detail of thermodynamic modeling. See DOI: 10.1039/x0xx00000x

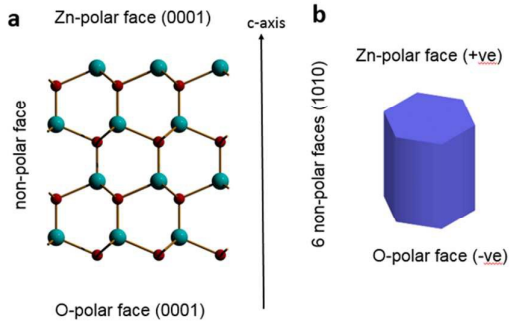

Figure 1 (a) The Zn-polar, O-polar and non-polar faces in ZnO wurtzite structure. (b) The Zn-polar, O-polar and non-polar faces in ZnO nanocrystal along c-axis

between the negative charged $Zn(OH)_4^{2-}$ complex ions and the positively charged Zn-polar top surface promoted the axial growth in the Zn-polar direction. Second, Chu et al. [8] pointed out that ZnO nanorods are O-polar because they can be etched into nanotubes by KOH, and the instability of the O-polar face that has been widely studied in many reports[20-22]. Third, Guillemin et al.[23] and Consoni et al.[24] have recently argued that the zinc oxide growth direction can be along the <000$\bar{1}$> O-polar direction as well as the <0001> Zn-polar direction even in the same hydrothermal condition. This is considered possible because the growth direction of ZnO is determined by the polarity of seed layer of ZnO quantum dots, which has random directions of the polarity after spin coating.

In this study, we fabricated ZnO nanorods by hydrothermal processes at different pH values. Then etched the nanorods using HCl and KOH solution to investigate their growth mechanism and the formation mechanism of the nanotubes. Valence band x-ray photoemission spectroscopy (VB-XPS) has been employed to examine the polarity of the nanorods. We found that nanorods formed in both acidic and alkaline solution are all Zn-polar. This finding led us to the fact that the surface energy of ZnO nanorods is another key factor in the formation of nanotubes.

Experimental

Materials and methods

ZnO quantum dot preparation

ZnO quantum dots were prepared in hydrolysis process[25]. 0.59g zinc acetate dehydrate (ZnAc) in 25ml methanol and 0.30g KOH in 13ml methanol were prepared separately. The ZnAc solution was heated with stirring at 65°C. Then, the KOH solution was added drop-wise into ZnAc solution over about 15min. After that, the time of reaction was 2.5hr. The ZnO QD was separated from solution by centrifugation. The precipitate was washed twice by adding methanol and then was centrifuged. Finally, the ZnO quantum dots were dispersed in the solution of n-butanol (14ml), methanol (1ml) and chloroform (1ml). The ZnO quantum dots solution was filtered through a 0.2um PVDF syringe filter and then dispersed again by ultrasonic before use.

ZnO nanorods fabrication

2.97g (100mM) zinc nitrate ($ZnNO_3$) and 1.40g (100mM) hexamethylenetetramine (HMTA) were added in the 100mL water. The pH values of mixture were adjusted by HCl or NH_3. The quantum dots were spin-coated on the ITO/glass substrates. The substrates were immersed in a chemical bath at 70°C, without stirring for 3 hours.

Structural and optical characterization

The nanostructure of the samples was examined by using field-emission scanning electron microscopy (FE-SEM, JSM-6700F and JSM-7100F).

X-ray photoemission spectroscopy

The Valence band XPS was investigated using the photoelectron spectrometer (AXIS Ultra DLD of Kratos).

Results and discussion

To study the growth mechanism of the ZnO nanostructures, we fabricated the nanorods by hydrothermal process at different pH values. Zinc oxide nanoparticles were spin-coated on the ITO glass substrate to form the seed layer. First, 100mM equal molar concentration of zinc nitrate ($ZnNO_3$) and hexamethylenetetramine (HMTA) were added to the chemical bath. Then, the pH values of chemical baths were adjusted by either hydrochloric acid (HCl) or ammonia (NH_3). The substrates were face-down and inclined 45° and immersed in the chemical bath at 70°C, without stirring for 3 hours. The ZnO nanorods substrates were rinsed with water afterward, then were etched with either 0.19M HCl at room temperature, or 0.3M KOH at 80 °C. The acid etching process has been widely studied, as it is a simple way to determine the polarity of ZnO, by examining the etching rates and the etched morphologies[21,26,27].

The Etching Study of ZnO nanorods

The morphologies of nanorods can be categorized into two types: the nanorods in the acidic growth conditions (NR_{acidic}) and those in the alkaline growth conditions ($NR_{alkaline}$). The zinc nitrate solution is slightly acidic, so it mixed with the weak base of HMTA in the chemical bath to reach a pH value of 6.4. The acidic growth conditions can be achieved by adjusting the concentration of HCl in the solution of 100mM equal molar $ZnNO_3$ and HMTA. The as-grown nanorods of acidic growth condition at the pH value of 6.4 usually had flat top surfaces, as shown in Figure 2a-b. The KOH etching process was achieved using 0.3M KOH solution at 80 °C for 30mins. After KOH etching, the nanorods became nanotubes (Figure 2c). Chu et al.[8] also reported such a finding. The nanorods fabricated in the acidic conditions at pH5.1-6.4 had similar morphologies after KOH etching (Figure S1), so we referred to these nanorods as NR_{acidic}. The HCl etching process was carried out

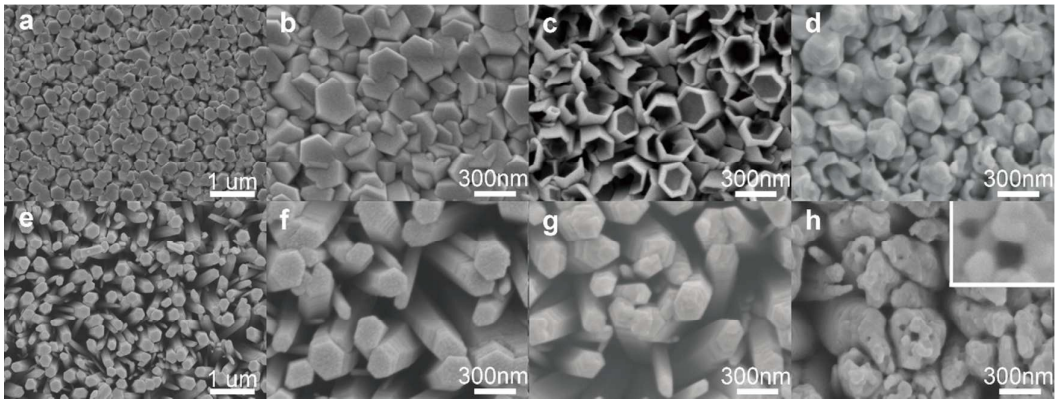

Figure 2 SEM images of the morphologies of ZnO. (a-d) Acidic growth condition (adjusted pH 6.4 by adding HCl). As-grown morphology of (a) low magnification, (b) high magnification. Etched morphologies (c) after 0.3M KOH etching at 80°C for 30mins, (d) after 0.19M HCl etching at room temperature for 15s. (e-h) Alkaline growth condition (adjusted pH 10.32 by adding NH3). As-grown morphology of (e) low magnification, (f) high magnification. Etched morphologies of (g) after 0.3M KOH etching at 80°C for 30mins, (h) after 0.19M HCl etching at room temperature for 15s.

by dipping the samples into 0.19M HCl at room temperature for 15s. After etching, the top of the nanorods became rough (Figure 2d). In alkaline growth conditions, we adjusted the pH by varying the concentration of NH_3 in the solution. The morphology of the nanorods shown in Figure 2e-f was achieved by the alkaline growth condition by adding 1.2M NH_3 at a pH value of 10.32. The as-grown nanorods of alkaline growth condition were obelisk-like, which is a similar result to that obtained by Wang et al.[28]. After the KOH etching process, the top surface of the as-grown $NR_{alkaline}$ were not etched into nanotubes (Figure 2g), in contrast to NR_{acidic}. The nanorods fabricated in alkaline conditions at pH9.8-10.32 had similar morphologies after KOH etching (Figure S1), so we referred to these nanorods as $NR_{alkaline}$ (Figure S2). After HCl etching, many hexagonal pits appeared on the top surface of the nanorods (Figure 2h). After etching, the difference in morphologies between NR_{acidic} and $NR_{alkaline}$ was easily observed. Consequently, the NR_{acidic} are easily constructed to be O-polar, because the O-polar face is less stable than the Zn-polar one. However, we will show that there is another reason, rather than the instability of O-polar, to explain the formation of nanotubes from nanorods.

However, the difference between the two conditions was eliminated after NR_{acidic} has been annealed at 450 °C for 15mins. Many small hexagonal pits appeared on the surfaces of annealed nanorods after HCl etching, as shown in Figure 3a. Scanning tunneling microscope (STM) images have been studied by O. Dulub et. al., G. Kresse et. al. and others indicating that there is surface reconstruction at the atomic level, thus increasing the stability of both of Zn- and O-polar faces after exposure to high temperature. The surface reconstruction of the Zn-polar face is very different from the O-polar face[13,29-32]. At the atomic level, many Zn-deficient triangular pits were formed on the Zn-polar face, whereas honeycomb structures were formed on the O-polar one.

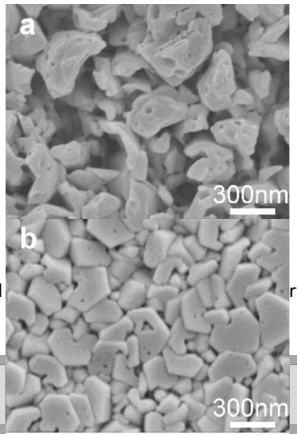

Figure 3. (a) SEM image of the morphology showing many small hexagonal pits after HCl etching of the annealed ZnO nanorods of acidic growth condition (annealed at 450°C for 15mins). (b) SEM image of the morphology showing many small hexagonal pits after KOH etching of the annealed ZnO nanorods of acidic growth condition.

Contrary to the instability of the O-polar face, at this juncture the annealed NR_{acidic} could not be etched into nanotubes by KOH.[33] The annealed NR_{acidic} were similar to the as-grown $NR_{alkaline}$, neither could be etched by KOH, as shown in Figure 3b. In bulk ZnO single crystal, the hexagonal pits were observed on Zn-polar surfaces after acidic etching[21,26,27]. It is suggested that nanorods of both conditions might be Zn-polar. The instability of O-polar was apparently not be the only cause of the formation of nanotubes. The Zn-polar nanorods could be etched into nanotubes also well, because large hexagonal pits can be observed after KOH etching on the O- and Zn-polar surface [22]. A direct measurement on the polarity of ZnO nanorods were needed in further investigation.

The Etching Study of ZnO nanoparticles

The previous discussion is based on the heterogeneously-grown ZnO nanorods. We further investigated the ZnO nanoparticles grown by the process of homogenous nucleation in the acidic and alkaline baths, at pH 6.4 and pH 10.32 respectively. The nanoparticles consisted of several nanorods growing from a nucleation site. A better description of homogeneously-grown and heterogeneously-grown ZnO has been shown in Figure S3. The SEM images of nanoparticles of the acidic growth condition at the pH value of 6.4 are shown in Figure 4a-b. Hollowed tubes were formed by KOH etching (Figure 4a), and the flat top surfaces became rough by HCl etching (Figure 4b). Other SEM images of nanoparticles of the alkaline growth condition at the pH value of 10.32 are shown in Figure 4c-d. During KOH etching, the dissolution began at the center of the ZnO nanoparticle (Figure 4c). After HCl etching, the surfaces which were exposed to solution became rough (Figure 4d). For heterogeneously-grown ZnO nanorods, the polarity can be controlled by the seed layer[23,24,34,35]. In contrast, the polarity of homogenously-grown ZnO nanoparticles was not limited by that. It is possible that the nanorods were in either the Zn-polar or O-polar direction. Several nanorods were grown from a nucleation site and each of them exhibited the same etching behavior. The growth directions of each nanorod were the same. The homogenously-grown ZnO nanorods show similarity in etching behaviors with the heterogeneously-grown nanorods. Therefore, we suggested that the growth directions of heterogeneously-grown nanorods were the same. To verify that, we examined the cross-section SEM of the nanorods after HCl etching, as shown in Figure 5. The etching rate of the O-polar face is much faster than that of the Zn-polar face as has been known by studies of HCl etching of ZnO single crystal[21,26,27]. If the nanorods are mix-polar, the etching rate of the Zn-polar and O-polar faces should be different. We measured the etching rate of ZnO fabricated in acidic and alkaline bath respectively. The growth rate of the $NR_{alkaline}$ was much faster than that of NR_{acidic}, so the longer NR_{acidic} has been fabricated by 3 times deposition before HCl etching. The result showed that the $NR_{alkaline}$ and NR_{acidic} have the similar etching rates about 30-40nm/s. More consequence to the polarity of ZnO, the etching rate of each nanorod is same to its neighboring ones. That implies the polarity of nanorods is unique in the same growth condition.

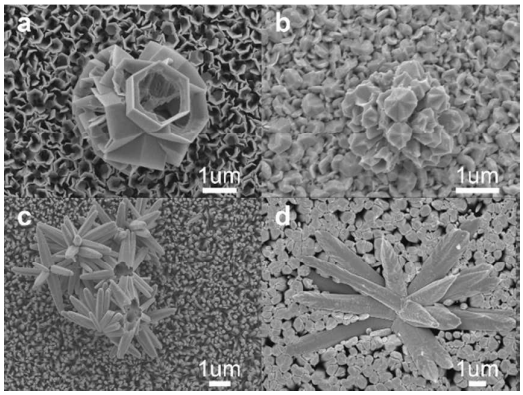

Figure 4 SEM images of the nanoparticles of ZnO. (a-b) The nanoparticles grown in acidic growth condition (a) after KOH etching, (b) after HCl etching. (c-d) The nanoparticles grown in alkaline growth condition (c) after KOH etching, (d) after HCl etching.

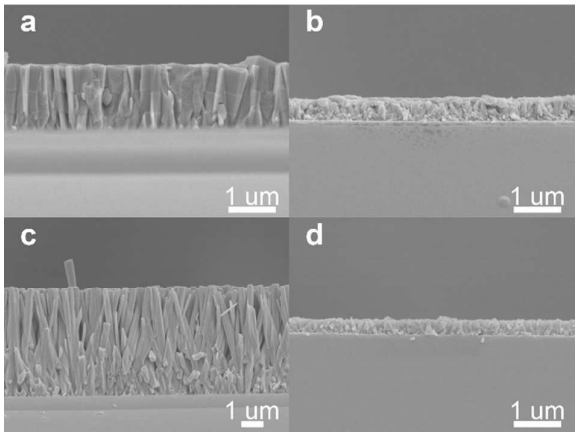

Figure 5. Cross section SEM images of ZnO nanorods. (a-b) Acidic growth condition. (a) As-grown 3 times chemical bath depositions. (b) After HCl etching for 120s. (c-d), Alkaline growth condition. (c) As-grown. (d) After HCl etching for 30s.

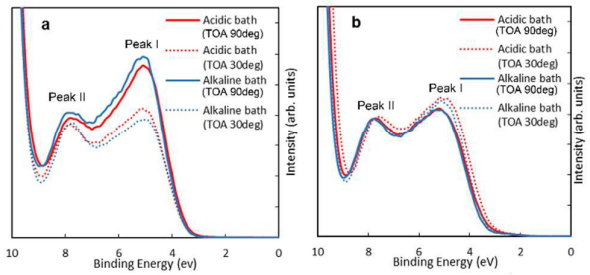

Figure 6 Valence XPS spectrum. (a) Valence band XPS spectrum by emitting Al K on the top surface. (Red solid line indicate the as-grown ZnO from acidic bath with TOA 90 deg, red dash line is that of with TOA 30 deg, blue solid line indicate the as grown ZnO from alkaline bath, blue dash line is that of with TOA 30 deg.) (b) Valence band XPS spectrum from emitting Al K on the bottom surface. (Red solid line indicate the as-grown ZnO from acidic bath with TOA 90 deg, red dash line is that of with TOA 30 deg, blue solid line indicate the as grown ZnO from alkaline bath, blue dash line is that of with take angle 30 deg).

The Polarity-related effects

Recently, Allen et al.[36,37] found that the valence band x-ray photoemission spectroscopy (VB-XPS) is a very useful way to determine the polarity of ZnO. The monochromatic Al K_α radiation (hv=1486.6eV) had been employed for this measurement. The spectra were normalized for comparison between the top layers and the bottom layers with two take-

off angles (TOAs) of 30° and 90°. There are two peaks in both Figure 6a and 6b. Peak I at around 5eV is related to predominately O 2p derived states. Peak II at around 7eV is attributed to hybridized states of O 2p, Zn 4s, and (possibly) Zn 3d character[38,39]. The VB-XPS has been employed to identify the Zn-polar face in the ZnO single crystal and thin film[40,41]. In these studies, the intensity of Peak I was significantly higher than that of Peak II on the Zn-polar face, but the intensity of two peaks was the same on the O-polar face. The result illustrated the polarity effect at the take-off angle (TOA) 90°. In our measurement, the intensity of Peak I is significantly higher than that of peak II on the top surfaces of NR_{acidic} and $NR_{alkaline}$, as shown in Figure 6a. It implies that the growth directions of both NR_{acidic} and $NR_{alkaline}$ are Zn-polar. At TOA of 30°, the polarity effect disappeared. It is important to note that the polarity effect is not affected by surface roughness, surface contamination and defect concentration[40]. The polarity effect is only sensitive to the Zn-polar direction.

The VB-XPS spectra had also been measured on the bottom sides of both NR_{acidic} and $NR_{alkaline}$, as shown in Figure 6b. We applied the epoxy on the top surfaces of them. Then, glass slides was put on the top surfaces to bond with the epoxy. The epoxy was cured at 100°C for 15mins. Finally, the thin films of ZnO nanorods were peeled off mechanically. To remove the seed layers of mix-polar quantum dots, the exposed bottom sides were etched using HCl solution for 2s. At both take-off angles of 30° and 90°, the intensity of peak II and Peak I are nearly same on the bottom sides of both NR_{acidic} and $NR_{alkaline}$ (Figure 6b). It implied that the bottom sides were O-polar. We ruled out the possibility the nanorods were mix-polar. As the measurement of the HCl etching rates showed, the growth direction should be unique in same chemical bath, as shown in Figure 5.

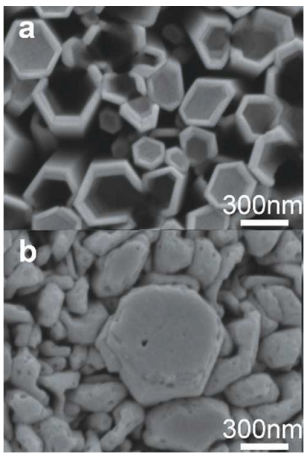

Figure 7 SEM image of the KOH etched morphology of ZnO (a) fabricated in two steps process: first 3 hours in alkaline bath then 1 hour in acidic bath; (b) fabricated in three steps process: first 3 hours in acidic bath, then annealing at 450°C for 15mins, and finally 1 hour in acidic bath.

Surface Energy

The nanorods of acidic and alkaline baths were confirmed to be Zn-polar. For the homogeneously-grown nanoparticle in the alkaline condition, the formation of nanotubes was due to the instability of the O-polar face. (Figure 4C) For the nanorods of heterogeneous growth, that will be caused by another factor. We suggested that the surface energy of as-grown $NR_{alkaline}$ ($S.E._{alkaline}$) was lower and more stable than NR_{acidic} ($S.E._{acidic}$) so that as-grown $NR_{alkaline}$ cannot be etched by KOH. The surface energy of annealed NR_{acidic} ($S.E._{annealed}$) became much more stable due to the surface reconstruction after exposure to high temperature. (Figure 3) The surface energy of NR_{acidic} bath was the highest and, in other words, unstable that the nanorods were easily etched into nanotubes. ($S.E._{acidic}$ > $S.E._{alkaline}$ > $S.E._{annealed}$) It is important to note that the comparison of surface energies of nanorods is only applied in KOH etching solution, as the presence of different solution can drastically affect the surface energies. We attempted to increase the surface energy of the $NR_{alkaline}$ and the annealed NR_{acidic}, by applying a second chemical deposition of acidic bath to these two samples. We expected that they could be etched into nanotubes. For the case of the as-grown $NR_{alkaline}$, the surface energy can be increased after the second acidic bath. Then, the nanotubes were formed. However, for the case of annealed NR_{acidic}, no nanotube was formed. It might have resulted from the vigorous surface reconstruction of the annealed surface that even affected the surface energy of the second ZnO layer.

Thermodynamics Modelling

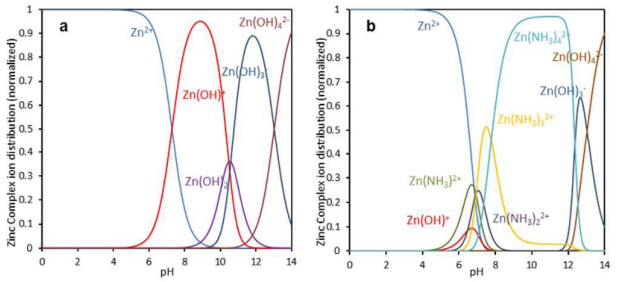

Figure 8 Thermodynamic modeling (predominance) of the ZnO hydrothermal process. (a) The distribution zinc complex ions in acidic bath at 70°C (b) The distribution zinc complex ions in alkaline bath at 70°C with 1.2M NH_3.

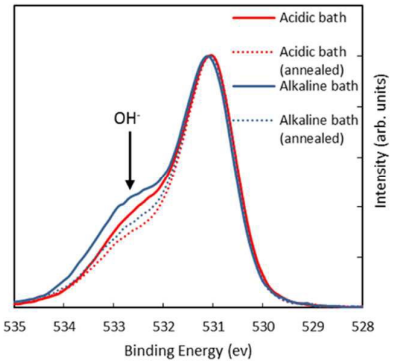

Figure 9 XPS O 1s core spectrum. (Red solid line indicate the as-grown ZnO from acidic bath, red dash line is that of after annealed, blue solid line indicate the as grown ZnO from alkaline bath, blue dash line is that of after annealed.)

CBD conditions	Atomic composition (%)			
	Zn	O	C	Zn/O
Acidic bath	41.31	47.53	11.16	0.87
Acidic bath (Annealed)	42.7	45.47	1.46	0.94
Alkaline bath	42.04	47.5	11.83	0.89
Alkaline bath (Annealed)	43.48	45.83	1.7	0.95

Table 1 Atomic composition of ZnO

We have further calculated the thermodynamic models of the Zn-OH and Zn-NH_3-OH system respectively. In the calculation, we adopted the data of the stability constant and the solubility production from Hubert et al.[42] and Goux et al.[19], as shown in Supporting Information. The HMTA is merely a weak base providing OH^- ions to react with Zn^{2+} ions. Therefore, for the acidic bath conditions, the Zn-OH system was considered. This is a plot of zinc complex ions distribution with five species that are Zn^{2+}, $Zn(OH)^+$, $Zn(OH)_2$, $Zn(OH)_3^{2-}$, and $Zn(OH)_4^{4-}$, as shown in Figure 8a. At the pH value of 6.4, the dominate complex ions are the Zn^{2+} complex ions. For the alkaline conditions, the Zn-NH_3-OH system was considered because NH_3 was added, as shown in Figure 8b. There are four more species that are $Zn(NH_3)^{2+}$, $Zn(NH_3)_2^{2+}$, $Zn(NH_3)_3^{2+}$ and $Zn(NH_3)_4^{2+}$, due to the Zn^{2+} combine with NH_3. At the pH value of 10.32, the $Zn(NH_3)_4^{2+}$ complex ions dominate. The $Zn(NH_3)_4^{2+}$ and Zn^{2+} ions are positive, but the NR_{acidic} and $NR_{alkaline}$ grows in Zn-polar direction. These positive ions cannot be attracted by the positive charged Zn-polar surfaces, due to electrostatic repulsion. In the growth mechanism of ZnO nanorods, OH^- ions are the key. X-ray photoemission (XPS) O 1s core spectrum has been confirmed to show the existence of OH^- dangling bonds on the Zn-polar surfaces.[30] The atomic composition has also been measured by XPS, as shown in Table 1. Before annealing, the Zn/O ratio was much lower in the as-grown nanorods of acidic and alkaline conditions. The reason is that the polar faces absorbed OH^- ligands and water molecules (or organic groups), lowering the Zn/O ratio. After annealing, the atomic composition of the both samples became close to 1:1. The O 1s XPS spectra also showed that the signal of OH group (532.3eV) dropped after annealing, as shown in Figure 9[30,37]. Therefore, we suggested that the growth mechanism of Zn-polar ZnO is achieved by the attraction of OH^- ions to positive Zn-polar face first. Then a negative OH^- layer forms to attract the positive Zn complex ions[7]. The reaction should be as followings:

$$Zn^{2+} + 2OH^- \rightleftharpoons ZnO + H_2O \quad (1)$$

$$Zn(NH_3)_4^{2+} + 2OH^- \rightleftharpoons ZnO + 4NH_3 + H_2O \quad (2)$$

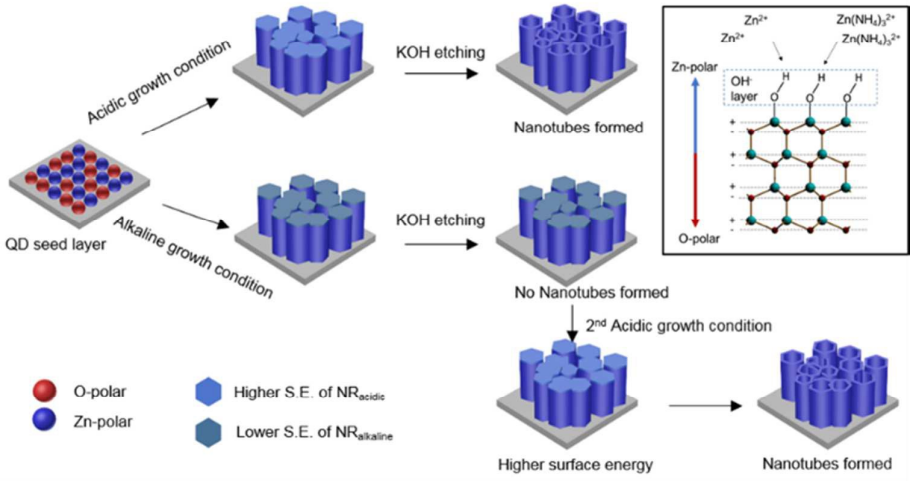

Figure 10 (a) The schematic diagram of ZnO growth mechanism of nanorods and transformation of nanotubes. (b)The electrostatic attraction of ions during the chemical reaction. The negative charged OH^- layer attracts the positive zinc complex ions, Zn^{2+} for acidic growth condition and $Zn(NH_3)_4^{2+}$ in alkaline growth condition, to form ZnO.

A schematic diagram of ZnO growth mechanism of nanorods and transformation of nanotubes is presented in Figure 10a. The quantum dots has random orientation in polarity in the seed layer. The Zn-polar nanorods have been developed via the faster growth rate in the growth completion between Zn-polar and O-polar. We also proposed that the formation of nanotubes after KOH etching depends on the high surface energy of nanorod, which can be achieved by acidic chemical bath deposition. The Zn-polar surface is positive charged which attracts the OH^- ions onto it to become a negative charge layer. After that, positive charged zinc complex ions are attracted onto the OH^- layer to form ZnO. The electrostatic attraction of ions has been shown in Figure 10b.

Conclusions

In summary, we have demonstrated the growth mechanism of ZnO nanorods in the hydrothermal process. The polarity plays an important role which influences growth direction, morphologies of ZnO nanostructures and the chemical reactions on the polar surfaces. It is important to identify NR_{acidic} and $NR_{alkaline}$ were Zn-polar. Therefore, we figured out that the surface energy of nanorods is also a key factor of the formation of nanotubes, besides the instability of the O-polar face. There were many studies about the method of controlling the aspect ratio of ZnO nanorods. In our experiment, we found that the $NR_{alkaline}$ has higher aspect ratio and faster growth rate than NR_{acidic}. By controlling the surface energy that the high-aspect-ratio $NR_{alkaline}$ could also be etched into nanotubes, we could have greater degree of freedom to manipulate the morphology of ZnO.

Acknowledgements

This work was funded by the State Key Laboratory on Advanced Displays and Optoelectronics Technologies (PSKL). We also gratefully thanks Paul Heinington for the discussion on this project and Nick K.C. Ho for the operation of VB-XPS.

Notes and references

1 Joo, J.; Chow, B. Y.; Prakash, M.; Boyden, E. S.; Jacobson, J. M. Face-Selective Electrostatic Control of Hydrothermal Zinc Oxide Nanowire Synthesis. *Nat. Mater.* **2011**, *10*, 596-601.
2 Jiang, Y.; Chen, S.; Li, G.; Li, H.; Kwok, H. A Low-Cost Nano-Modified Substrate Integrating both Internal and External Light Extractors for Enhancing Light Out-Coupling in Organic Light-Emitting Diodes. *Adv. Opt. Mater.* **2014**, *2*, 418-422.
3 Sharma, P.; Gupta, A.; Owens, F. J.; Inoue, A.; Rao, K. V. Room Temperature Spintronic Material—Mn-Doped ZnO Revisited. *J. Magn. Magn. Mater.* **2004**, *282*, 115-121.
4 Chen, R.; Zhou, W.; Zhang, M.; Kwok, H. S. High Performance Self-Aligned Top-Gate ZnO Thin Film Transistors Using Sputtered Al_2O_3 Gate Dielectric. *Thin Solid Films* **2012**, *520*, 6681-6683.
5 Wang, Z. L.; Song, J. Piezoelectric Nanogenerators Based on Zinc Oxide Nanowire Arrays. *Science* **2006**, *312*, 242-246.
6 Son, D.; Im, J.; Kim, H.; Park, N. 11% Efficient Perovskite Solar Cell Based on ZnO Nanorods: An Effective Charge Collection System. *J. Phys. Chem. C* **2014**, *118*, 16567-16573.
7 Li, F.; Ding, Y.; Gao, P.; Xin, X.; Wang, Z. L. Single-Crystal Hexagonal Disks and Rings of ZnO: Low-Temperature, Large-Scale Synthesis and Growth Mechanism. *Angewandte Chemie International Edition* **2004**, *43*, 5238-5242.
8 Chu, D.; Masuda, Y.; Ohji, T.; Kato, K. Formation and Photocatalytic Application of ZnO Nanotubes Using Aqueous Solution. *Langmuir* **2009**, *26*, 2811-2815.
9 Golovko, D. S.; Muñoz-Espí, R.; Wegner, G. Interaction between Poly(styrene-acrylic acid) Latex Nanoparticles and Zinc Oxide Surfaces. *Langmuir* **2007**, *23*, 3566-3569.
10 Allen, M.; Miller, P.; Reeves, R.; Durbin, S. Influence of Spontaneous Polarization on the Electrical and Optical Properties of Bulk, Single Crystal ZnO. *Appl. Phys. Lett.* **2007**, *90*, 062104-062104-3.
11 Allen, M.; Mendelsberg, R.; Reeves, R.; Durbin, S. Oxidized Noble Metal Schottky Contacts to N-type ZnO. *Appl. Phys. Lett.* **2009**, *94*, 103508.
12 Dulub, O.; Boatner, L. A.; Diebold, U. STM Study of the Geometric and Electronic Structure of ZnO (0001)-Zn, (0001)-O, (1010), and (1120) surfaces. *Surf. Sci.* **2002**, *519*, 201-217.
13 Dulub, O.; Diebold, U.; Kresse, G. Novel Stabilization Mechanism on Polar Surfaces: ZnO (0001)-Zn. *Phys. Rev. Lett.* **2003**, *90*, 016102.
14 Li, W.; Shi, E.; Zhong, W.; Yin, Z. Growth Mechanism and Growth Habit of Oxide Crystals. *J. Cryst. Growth* **1999**, *203*, 186-196.
15 Laudise, R.; Ballman, A. Hydrothermal Systhesis of Zinc Oxide and Zinc Sulfide[1]. *J. Phys. Chem.* **1960**, *64*, 688-691.
16 Richardson, J. J.; Lange, F. F. Controlling Low Temperature Aqueous Synthesis of ZnO. 1. Thermodynamic Analysis. *Cryst. Growth Des.* **2009**, *9*, 2570-2575.
17 Peterson, R. B.; Fields, C. L.; Gregg, B. A. Epitaxial Chemical Deposition of ZnO Nanocolumns from NaOH Solutions. *Langmuir* **2004**, *20*, 5114-5118.
18 Yamabi, S.; Imai, H. Growth Conditions for Wurtzite Zinc Oxide Films in Aqueous Solutions. *J. Mater. Chem.* **2002**, *12*, 3773-3778.
19 Goux, A.; Pauporté, T.; Chivot, J.; Lincot, D. Temperature Effects on ZnO Electrodeposition. *Electrochim. Acta* **2005**, *50*, 2239-2248.
20 Mehta, M.; Meier, C. Controlled Etching Behavior of O-Polar and Zn-Polar ZnO Single Crystals. *J. Electrochem. Soc.* **2011**, *158*, H119-H123.
21 Han, S.; Kim, J.; Kim, J. Y.; Kim, K.; Tampo, H.; Niki, S.; Lee, J. Formation of Hexagonal Pyramids and Pits on V-/VI-Polar and III-/II-Polar GaN/ZnO Surfaces by Wet Etching. *J. Electrochem. Soc.* **2010**, *157*, D60-D64.
22 Nicholas, N. J.; Ducker, W.; Franks, G. V. Differential Etching of ZnO Native Planes under Basic Conditions. *Langmuir* **2012**, *28*, 5633-5641.
23 Guillemin, S.; Rapenne, L.; Roussel, H.; Sarigiannidou, E.; Brémond, G.; Consonni, V. Formation Mechanisms of ZnO Nanowires: the Crucial Role of Crystal Orientation and Polarity. *J. Phys. Chem. C* **2013**, *117*, 20738-20745.
24 Consonni, V.; Sarigiannidou, E.; Appert, E.; Bocheux, A.; Guillemin, S.; Donatini, F.; Robin, I.; Kioseoglou, J.; Robaut, F. Selective Area Growth of Well-Ordered ZnO Nanowire Arrays with Controllable Polarity. *ACS Nano* **2014**.
25 Wang, Z.; Qian, X.; Yin, J.; Zhu, Z. Aqueous Solution Fabrication of Large-Scale Arrayed Obelisk-Like Zinc Oxide Nanorods with High Efficiency. *J. Solid State Chem.* **2004**, *177*, 2144-2149.
26 Xu, H.; Dong, L.; Shi, X.; Van Hove, M.; Ho, W.; Lin, N.; Wu, H.; Tong, S. Stabilizing Forces Acting on ZnO Polar Surfaces: STM, LEED, and DFT. *Phys. Rev. B* **2014**, *89*, 235403.
27 Lauritsen, J. V.; Porsgaard, S.; Rasmussen, M. K.; Jensen, M. C.; Bechstein, R.; Meinander, K.; Clausen, B. S.; Helveg, S.; Wahl, R.; Kresse, G. Stabilization Principles for Polar Surfaces of ZnO. *ACS Nano* **2011**, *5*, 5987-5994.
28 Wahl, R.; Lauritsen, J. V.; Besenbacher, F.; Kresse, G. Stabilization Mechanism for the Polar ZnO (0001)-O Surface. *Phys. Rev. B* **2013**, *87*, 085313.
29 Kresse, G.; Dulub, O.; Diebold, U. Competing Stabilization Mechanism for the Polar ZnO (0001)-Zn Surface. *Phys. Rev. B* **2003**, *68*, 245409.
30 She, G.; Zhang, X.; Shi, W.; Fan, X.; Chang, J. C.; Lee, C.; Lee, S.; Liu, C. Controlled Synthesis of Oriented Single-Crystal ZnO Nanotube Arrays on Transparent Conductive Substrates. *Appl. Phys. Lett.* **2008**, *92*, 053111-053111-3.
31 Mariano, A.; Hanneman, R. Crystallographic Polarity of ZnO Crystals. *J. Appl. Phys.* **1963**, *34*, 384-388.
32 Tampo, H.; Fons, P.; Yamada, A.; Kim, K.; Shibata, H.; Matsubara, K.; Niki, S.; Yoshikawa, H.; Kanie, H. Determination of Crystallographic Polarity of ZnO Layers. *Appl. Phys. Lett.* **2005**, *87*, 141904.

33 Kato, H.; Miyamoto, K.; Sano, M.; Yao, T. Polarity Control of ZnO on Sapphire by Varying the MgO Buffer Layer Thickness. *Appl. Phys. Lett.* **2004**, *84*, 4562-4564.
34 Hong, S.; Hanada, T.; Ko, H.; Chen, Y.; Yao, T.; Imai, D.; Araki, K.; Shinohara, M.; Saitoh, K.; Terauchi, M. Control of Crystal Polarity in a Wurtzite Crystal: ZnO Films Grown by Plasma-Assisted Molecular-Beam Epitaxy on GaN. *Phys. Rev. B* **2002**, *65*, 115331.
35 Heinhold, R.; Allen, M. W. Polarity-Dependent Photoemission of In Situ Cleaved Zinc Oxide Single Crystals. *J. Mater. Res.* **2012**, *27*, 2214-2219.
36 Allen, M.; Zemlyanov, D.; Waterhouse, G.; Metson, J.; Veal, T. D.; McConville, C. F.; Durbin, S. Polarity Effects in the X-Ray Photoemission of ZnO and Other Wurtzite Semiconductors. *Appl. Phys. Lett.* **2011**, *98*, 101906-101906-3.
37 King, P.; Veal, T. D.; Schleife, A.; Zúñiga-Pérez, J.; Martel, B.; Jefferson, P.; Fuchs, F.; Muñoz-Sanjosé, V.; Bechstedt, F.; McConville, C. F. Valence-Band Electronic Structure of CdO, ZnO, and MgO from X-Ray Photoemission Spectroscopy and Quasi-Particle-Corrected Density-Functional Theory Calculations. *Phys. Rev. B* **2009**, *79*, 205205.
38 Göpel, W.; Pollmann, J.; Ivanov, I.; Reihl, B. Angle-Resolved Photoemission from Polar and Nonpolar Zinc Oxide Surfaces. *Phys. Rev. B* **1982**, *26*, 3144.
39 Williams, J.; Yoshikawa, H.; Ueda, S.; Yamashita, Y.; Kobayashi, K.; Adachi, Y.; Haneda, H.; Ohgaki, T.; Miyazaki, H.; Ishigaki, T. Polarity-Dependent Photoemission Spectra of Wurtzite-Type Zinc Oxide. *Appl. Phys. Lett.* **2012**, *100*, 051902.
40 Williams, J. R.; Furukawa, H.; Adachi, Y.; Grachev, S.; Søndergård, E.; Ohashi, N. Polarity Control of Intrinsic ZnO Films Using Substrate Bias. *Appl. Phys. Lett.* **2013**, *103*, 042107.
41 Hubert, C.; Naghavi, N.; Canava, B.; Etcheberry, A.; Lincot, D. Thermodynamic and Experimental Study of Chemical Bath Deposition of Zn(S,O,OH) Buffer Layers in Basic Aqueous Ammonia Solutions. Cell Results with Electrodeposited $CuIn(S,Se)_2$ Absorbers. *Thin Solid Films* **2007**, *515*, 6032-6035.
42 Liu, D.; Kelly, T. L. Perovskite Solar Cells with a Planar Heterojunction Structure Prepared Using Room-Temperature Solution Processing Techniques. *Nature Photon.* **2014**, *8*, 133-138.